

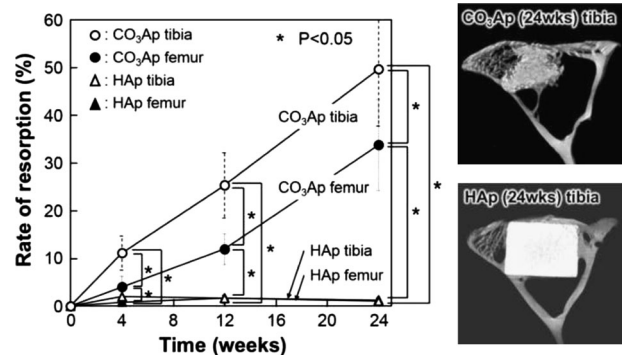
# Evaluation of carbonate apatite blocks fabricated from dicalcium phosphate dihydrate blocks for reconstruction of rabbit femoral and tibial defects

Masayuki Kanazawa<sup>1</sup> · Kanji Tsuru<sup>2</sup> · Naoyuki Fukuda<sup>2</sup> · Yuta Sakemi<sup>1</sup> · Yasuharu Nakashima<sup>1</sup> · Kunio Ishikawa<sup>2</sup>

Received: 26 November 2016 / Accepted: 22 April 2017 / Published online: 29 April 2017  
© Springer Science+Business Media New York 2017

**Abstract** This study aimed to evaluate in vivo behavior of a carbonate apatite (CO<sub>3</sub>Ap) block fabricated by compositional transformation via a dissolution–precipitation reaction using a calcium hydrogen phosphate dihydrate [DCPD: CaHPO<sub>4</sub>·2H<sub>2</sub>O] block as a precursor. These blocks were used to reconstruct defects in the femur and tibia of rabbits, using sintered dense hydroxyapatite (HAp) blocks as the control. Both the CO<sub>3</sub>Ap and HAp blocks showed excellent tissue response and good osteoconductivity. HAp block maintained its structure even after 24 weeks of implantation, so no bone replacement of the implant was observed throughout the post-implantation period in either femoral or tibial bone defects. In contrast, CO<sub>3</sub>Ap was resorbed with increasing time after implantation and replaced with new bone. The CO<sub>3</sub>Ap block was resorbed approximately twice as fast at the metaphysis of the proximal tibia than at the epiphysis of the distal femur. The CO<sub>3</sub>Ap block was resorbed at an approximately linear change over time, with complete resorption was estimated by extrapolation of data at approximately 1–1.5 years. Hence, the CO<sub>3</sub>Ap block fabricated in this study has potential value as an ideal artificial bone substitute because of its resorption and subsequent replacement by bone.

## Graphical Abstract



## 1 Introduction

Bone graft materials are necessary during orthopedic surgery, such as for critically sized bone defects or in the presence of pseudarthrosis. Autogenous bone grafts are still the gold standard for bone replacement because they have displayed osteoconduction, osteoinduction, and osteogenesis without causing an immunologic response [1–3]. Additional incisions in healthy skin, however, are needed for that technique [4]. Furthermore, it is difficult to reconstruct bone tissue in large defects using only autogenous bone grafts because of the limited amount of available bone. In such cases, artificial bone substitutes are utilized.

Clinically, hydroxyapatite (HAp) [Ca<sub>10</sub>(PO<sub>4</sub>)<sub>6</sub>(OH)<sub>2</sub>] has been commonly used as an artificial bone substitute because of its excellent tissue response and osteoconductivity [1–3, 5–7]. After implantation in bone defect, however, HAp remains at the implant site for a long time [1, 8]. Such

✉ Kanji Tsuru  
tsuru@dent.kyushu-u.ac.jp

<sup>1</sup> Department of Orthopaedic Surgery, Graduate School of Medical Sciences, Kyushu University, 3-1-1 Maidashi, Higashi-ku, Fukuoka 812-8582, Japan

<sup>2</sup> Department of Biomaterials, Faculty of Dental Science, Kyushu University, 3-1-1 Maidashi, Higashi-Ku, Fukuoka 812-8582, Japan

remaining artificial bone substitute, although without immune function, is associated with a risk of infection [9]. Therefore, a resorbable apatite bone substitute has been sought. Carbonate apatite [ $\text{CO}_3\text{Ap}$ :  $\text{Ca}_{10-a}(\text{CO}_3)_b(\text{PO}_4)_{6-c}(\text{OH})_{2-d}$ ] artificial bone substitute [9–15] is closer to natural bone than HAp because bone apatite also contains carbonate in its apatitic structure [16]. This synthetic  $\text{CO}_3\text{Ap}$  bone substitute has the potential to be an ideal bone substitute that is gradually replaced by new bone during a bone-remodeling cycle [9].

A  $\text{CO}_3\text{Ap}$  bone substitute can be fabricated by compositional transformation via a dissolution–precipitation reaction using a precursor. To date, a calcite ( $\text{CaCO}_3$ ) block [9, 10], a calcium sulfate ( $\text{CaSO}_4$ ) block [11, 12], and an  $\alpha$ -tricalcium phosphate ( $\alpha$ -TCP) block [13–15] have been used as precursors for fabricating the  $\text{CO}_3\text{Ap}$  block.

Recently, dicalcium phosphate dihydrate [DCPD:  $\text{CaH}_2\text{PO}_4 \cdot 2\text{H}_2\text{O}$ ] was found to be a satisfactory precursor for fabricating the  $\text{CO}_3\text{Ap}$  block [17]. The DCPD block can be fabricated based on the setting reaction of DCPD-forming cement. In other words, it is easy to create any shape of DCPD block. DCPD composition includes Ca and  $\text{PO}_4$  and is suitably soluble for the dissolution–precipitation reaction.

To date, however, there have been no studies regarding the *in vivo* behavior of  $\text{CO}_3\text{Ap}$  block fabricated from DCPD. Also, no comparison study has been performed to evaluate the rate at which the  $\text{CO}_3\text{Ap}$  block has been replaced by bone at various bone defect sites. In this study, therefore,  $\text{CO}_3\text{Ap}$  block fabricated from DCPD blocks and sintered HAp were implanted in femoral and tibial bone defects of rabbits. The sintered HAp block was employed as a typical, commercially available and non-resorbable bone substitute. The implants were examined using micro-computed tomography (CT) up to 24 weeks after implantation in 19 male rabbits.

## 2 Materials and methods

### 2.1 Preparation of cylindrical $\text{CO}_3\text{Ap}$ blocks

Cylindrical  $\text{CO}_3\text{Ap}$  blocks (6 mm diameter, 4 mm high) were fabricated via compositional transformation of cylindrical DCPD blocks, as described elsewhere [17]. First, the DCPD block was fabricated based on the setting reaction of DCPD forming cement [18–20].  $\beta$ -TCP [ $\beta$ - $\text{Ca}_3(\text{PO}_4)_2$ ] (Taihei Chemicals, Osaka, Japan) and monocalcium phosphate monohydrate [ $\text{Ca}(\text{H}_2\text{PO}_4)_2 \cdot \text{H}_2\text{O}$ ] (Sigma Aldrich, St. Louis, MO, USA) powders were mixed with methanol so the Ca/P molar ratio would be 1.0 (the molar ratio of DCPD). After the methanol was evaporated, the powder mixture was placed in a mold followed by a sufficient amount of water to set the block.

Second, composition of the DCPD precursor block was changed to  $\text{CO}_3\text{Ap}$  using compositional transformation via a dissolution–precipitation reaction. The DCPD block was immersed in  $\text{Na}_2\text{CO}_3$  solution (2 mol/L) at 80 °C for 14 days.

As a typical, commercially available and non-resorbable bone substitute, a cylindrical HAp block (6 mm diameter, 4 mm high) was prepared using the following procedure. HAp powder (HAP-200; Taihei Chemicals) was placed in a stainless steel mold and uniaxially pressed by loading 20 MPa using an oil pressure press machine (MT-50HD; NPa System, Saitama, Japan). The obtained, compacted material was then heated in an electronic furnace (SBV-1515D; Motoyama, Osaka, Japan) up to 1300 °C at 5 °C/min and then maintained at this temperature for 6 h, followed by cooling to room temperature inside the furnace.

### 2.2 Characterization of specimens

The obtained blocks were subjected to powder X-ray diffractometry (XRD) (D8 Advance; Bruker AXS GmbH, Karlsruhe, Germany) [ $\text{CuK}\alpha$  ( $\lambda = 0.1542$  nm), 40 kV, 40 mA] during continuous scanning from 10° to 40° at 2 $\theta$  at a scanning rate of 2°/min. Fourier transform infrared (FT-IR) spectra were measured with an FT-IR spectrometer (FT/IR-6200, JASCO, Tokyo, Japan) using KBr method. The spectral resolution of 4  $\text{cm}^{-1}$  was employed to examine structural changes.

The surface morphology of the obtained specimens was evaluated using a scanning electron microscopy (SEM) (S-3400N; Hitachi High-Technologies, Tokyo, Japan) at 15 kV accelerating voltage after applying a gold–palladium coating with a magnetron sputtering machine (MSP-1S; Vacuum Device Co., Ibaraki, Japan). The specific surface area (SSA) was measured using the Brunauer-Emmett-Teller (BET)  $\text{N}_2$  adsorption method (Gemini 2370; Micromeritics, Norcross, GA, USA). The porosity was calculated using the bulk density of the specimen ( $d_{\text{specimen}}$ ) and the theoretical density of HAp ( $d_{\text{HAp}}$  3.16  $\text{g}/\text{cm}^3$ ) [21], as shown in [Eq. 1].

$$\text{Porosity}(\%) = d_{\text{HAp}} - \frac{d_{\text{specimen}}}{d_{\text{HAp}}} \times 100 \quad (1)$$

Carbonate contents were estimated from the mass% of carbon in the  $\text{CO}_3\text{Ap}$  block. A CHN coder (MT-6; Yanako Analytical Instruments, Kyoto, Japan) was used to analyze the mass% of carbon.

### 2.3 Procedure for the animal experiment

A total of 19 Japanese white male rabbits (Japan SLC Inc., Hamamatsu, Japan) (age range 19–20 weeks; mean body

weight  $3335 \pm 322$  g) were studied. The animals were housed in the animal center of our institution and maintained on a standard diet and water. All experiments followed protocols that were approved by the Animal Care and Use Committee (Approval Number A-27-328-0, issued on March 16, 2016). The experiments were conducted in accordance with the Guidelines for Animal Experiments of our institution, Japanese law (No. 105), and notification No. 6 of the government of Japan.

Rabbits were anesthetized by intramuscular injection of ketamine-xylazine (35–10 mg/kg). The rear limb was shaved and then disinfected using iodine. To understand the effects of the location of bony tissue on the resorption of CO<sub>3</sub>Ap and HAp block specimens, we selected two sites for implantation. The epiphysis of the distal femur and metaphysis of the proximal tibia were employed because of the availability of sufficient bone volume and easy surgical exposure. A medial, longitudinal skin incision was made at each distal femur, and the medial femoral condyle was exposed. A 6.1-mm hole was drilled into the epiphysis of the distal femur, into which the block specimen was inserted. The fascia was then sutured. The next skin incision was in the proximal tibia. A similar 6.1-mm hole was drilled into the metaphysis of the proximal tibia and the block specimen inserted. In all rabbits used, both CO<sub>3</sub>Ap and HAp blocks were implanted bilaterally. All rabbits were allowed unrestrained movement in their cages after recovery from anesthesia. One rabbit was used for the collecting data for day 0. Day 0 means that samples with surrounding bone were collected just after the implantation ( $n = 1$  in each group). For other implantation periods, the rabbits were euthanized, in batches, at 4, 12, and 24 weeks after implantation, and the epiphyses of the distal femurs and metaphyses of the proximal tibias were harvested ( $n = 6$  in each group).

## 2.4 Micro-CT

The excised distal femur and proximal tibia with block specimens were scanned using micro-CT (Skyscan 1075 KHS; Skyscan, Kontich, Belgium) (source voltage 60 kV, source current 170  $\mu$ A, 0.5-mm aluminum filter). The samples were scanned using the high-resolution mode (9  $\mu$ m voxel resolution). Isotropic slice data were obtained from micro-CT measurements and reconstruction to two-dimensional images. These slice images were compiled and analyzed to render three-dimensional (3D) images using analyzing software. The volume of the residual block specimen was calculated using a quantitative 3D evaluation program that had been installed in an analytical personal computer [22]. Before implantation, the volume of each block specimen was calculated using its diameter and

height. The resorption rate (%) was calculated using [Eq. 2].

$$\text{Resorption rate (\%)} = 100 - \left( \frac{\text{volume of residual block specimen}}{\text{volume of block specimen before implantation}} \right) \times 100 \quad (2)$$

## 2.5 Statistical analysis

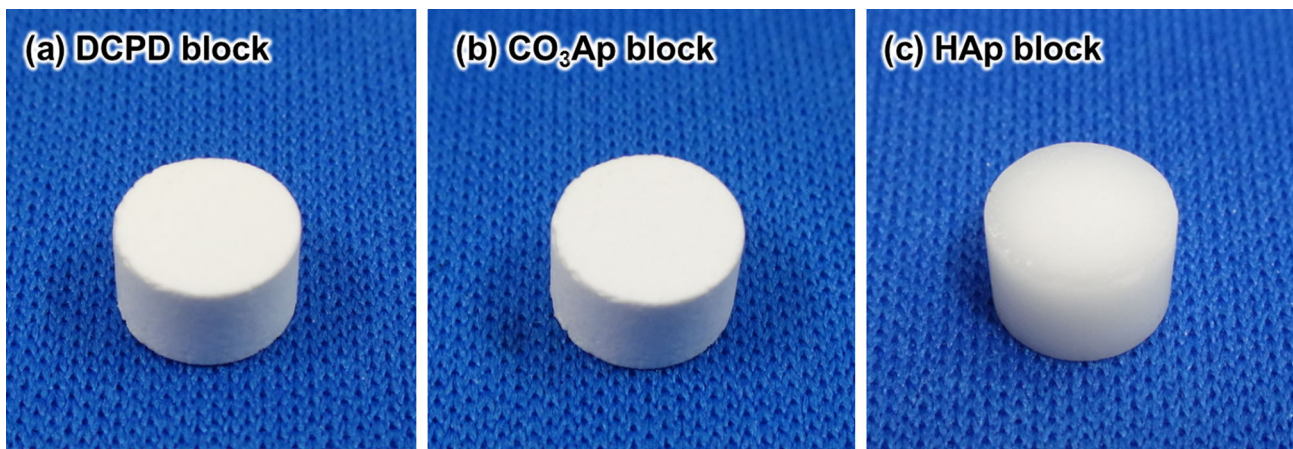
Resorption rates are expressed as means  $\pm$  SD. The Mann–Whitney U test was used to assess the difference in the resorption rates between the CO<sub>3</sub>Ap and HAp blocks. The differences in the resorption rates between the femur group and the tibia group were assessed in the same way. Statistical analyses were performed using JMP Software (version 11.0; SAS Institute, Cary, NC, USA). A probability value of  $<0.05$  was considered to indicate statistical significance.

## 3 Results

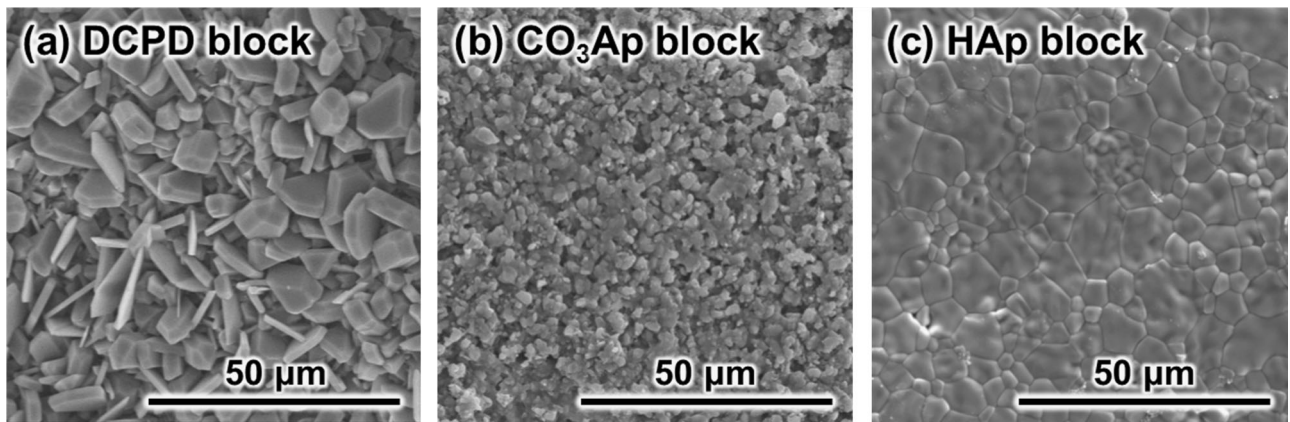
Figure 1 shows typical photographs of (a) a DCPD block used as a precursor for fabricating a CO<sub>3</sub>Ap block, (b) a CO<sub>3</sub>Ap block, and (c) an HAp block (used as the control). As shown, the size of the DCPD and CO<sub>3</sub>Ap cylindrical blocks (6 mm diameter, 4 mm high) were the same, indicating that the CO<sub>3</sub>Ap block fabricated by compositional transformation via a dissolution–precipitation reaction using DCPD as a precursor maintained its macroscopic structure. The DCPD and CO<sub>3</sub>Ap blocks had opaque bodies, whereas the HAp block had a relatively translucent body, which is typical for well-sintered ceramic creations.

Figure 2 shows typical SEM images of (a) a DCPD block, (b) a CO<sub>3</sub>Ap block, and (c) an HAp block. The DCPD block consists of plate-like crystals, whereas the CO<sub>3</sub>Ap block consists of small polygon-like crystals. In both cases, the crystals were interlocked, similar to those in set gypsum. This structure is typical for products made via a dissolution–precipitation reaction using a precursor. The different crystal morphologies indicated that compositional transformation via the dissolution–precipitation reaction maintained their macroscopic structure but not their microstructure. In contrast, sintered HAp showed a typical surface for sintered ceramic objects. In other words, grains and grain boundaries were seen on its surface.

Figure 3 shows the powder XRD patterns of (a) DCPD block used as a precursor for CO<sub>3</sub>Ap block fabrication, (b) CO<sub>3</sub>Ap block, and (c) HAp blocks. XRD patterns of (d) DCPD and (e) HAp are shown for comparison. XRD analysis demonstrated clearly that DCPD block completely transformed to a pure CO<sub>3</sub>Ap block without by-products.



**Fig. 1** Typical photographs of **a** a dicalcium phosphate dehydrate (DCPD) block used as a precursor for fabrication of a carbonate apatite ( $\text{CO}_3\text{Ap}$ ) block, **b**  $\text{CO}_3\text{Ap}$  block and **c** sintered hydroxyapatite (HAp) block (used as a control)



**Fig. 2** Typical scanning electron microscopy (SEM) micrographs of **a** DCPD block, **b**  $\text{CO}_3\text{Ap}$  block, and **c** HAp block

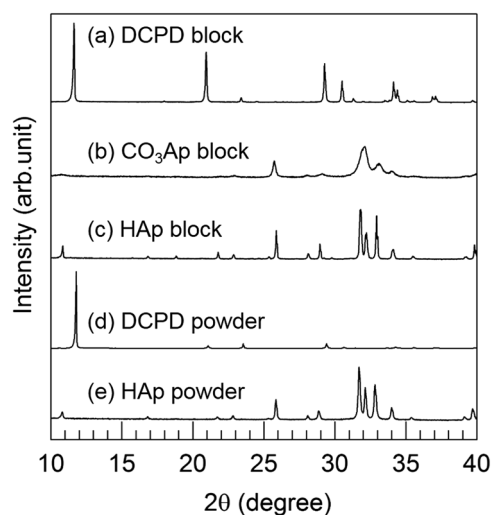


**Fig. 3** Powder X-ray diffractometry (XRD) patterns of **a** DCPD block, **b**  $\text{CO}_3\text{Ap}$  block, **c** HAp block. XRD patterns of **d** DCPD powder and **e** HAp powder were used for comparison

Peaks of  $\text{CO}_3\text{Ap}$  were broad, indicating that  $\text{CO}_3\text{Ap}$  with low crystallinity was formed. In contrast, sintered HAp showed sharp peaks, indicating high-crystallinity apatite. In this case as well, all peaks were attributed to HAp. The difference in crystallinity was based on the temperature needed for its fabrication.  $\text{CO}_3\text{Ap}$  block was fabricated at  $80^\circ\text{C}$  in aqueous solution, whereas sintered HAp was fabricated at  $1300^\circ\text{C}$ .

Figure 4 shows the FT-IR spectra for the (a) DCPD block used as a precursor for  $\text{CO}_3\text{Ap}$  block fabrication, (b)  $\text{CO}_3\text{Ap}$  blocks, and (c) HAp blocks. The FT-IR spectra of (d) DCPD and (e) HAp are shown for comparison. FT-IR spectra also confirmed a DCPD block transformed to a  $\text{CO}_3\text{Ap}$  block. The peaks at  $567$ ,  $606$ ,  $1042$ , and  $1092\text{ cm}^{-1}$  are assigned to  $\text{PO}_4^{3-}$  groups [23]; those at  $875$ ,  $1418$ , and  $1474\text{ cm}^{-1}$  are assigned to  $\text{CO}_3^{2-}$  groups [24]; and peaks at  $640\text{ cm}^{-1}$  are assigned to  $\text{OH}^-$  groups [23].  $\text{PO}_4^{3-}$  groups were observed for all DCPD,  $\text{CO}_3\text{Ap}$ , and HAp specimens, whereas  $\text{CO}_3^{2-}$  groups were observed only for the  $\text{CO}_3\text{Ap}$

specimens. OH<sup>-</sup> groups were observed for HAp but not for CO<sub>3</sub>Ap specimens. The peak positions of CO<sub>3</sub><sup>2-</sup> groups and absence of an OH<sup>-</sup> group imply that the obtained CO<sub>3</sub>Ap is similar to an AB-type carbonated apatite that has been reported in our previous paper [17]. In short, CO<sub>3</sub><sup>2-</sup> ions were substituted at both OH<sup>-</sup> and PO<sub>4</sub><sup>3-</sup> sites in the apatite crystal lattice and some of CO<sub>3</sub><sup>2-</sup> ions were adsorped on the surface of CO<sub>3</sub>Ap crystal [16, 24, 25]. The broad peaks at 1647 cm<sup>-1</sup> were relevant to H<sub>2</sub>O. No peak

near 1647 cm<sup>-1</sup> was observed from the HAp specimen because it was sintered at 1300 °C.

Table 1 summarizes the SSA, total porosity, and carbonate contents of the CO<sub>3</sub>Ap and HAp blocks. The porosity and SSA of the CO<sub>3</sub>Ap block were significantly higher than those of the HAp block. The CO<sub>3</sub>Ap block contained approximately 16 wt% CO<sub>3</sub><sup>2-</sup> groups, whereas the HAp block was free of these groups. CO<sub>3</sub>Ap block has an SSA of approximately 22 cm<sup>2</sup>/g, whereas that of the HAp block is very small. In other words, the value could not be measured based on the BET analysis. The porosity of the CO<sub>3</sub>Ap block was approximately 49%, which is approximately 10 times larger than that of the HAp block. This porosity is consistent with the SEM observation shown in Fig. 2.

Figure 5 shows the micro-CT images (side view of the cylindrical block) of the CO<sub>3</sub>Ap blocks (a–d) and HAp blocks (e–h) immediately after implantation (day 0) (a, e) and at 4 (b, f), 12 (c, g), and 24 (d, h) weeks after implantation in the rabbits' distal femurs. HAp maintained its structure even at 24 weeks after the operation. In other

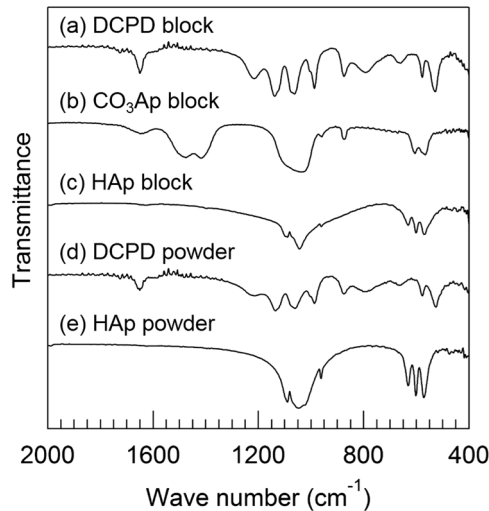


**Fig. 4** Fourier transform infrared (FT-IR) spectra of **a** DCPD block, **b** CO<sub>3</sub>Ap block, and **c** HAp block. FT-IR spectra of **d** DCPD powder and **e** HAp powder were used for comparison

**Table 1** Specific surface area (SSA), porosity, and carbonate contents of CO<sub>3</sub>Ap and HAp blocks used in this study

	SSA (cm <sup>2</sup> /g)	Porosity (%)	CO <sub>2</sub> contents (mol%)
CO <sub>3</sub> Ap block	22.4 ± 1.2	49.1 ± 1.9	15.8 ± 0.9
HAp block	u.d.*	4.7 ± 0.1	0

\*SSA value of HAp block was undetectable (u.d.) due to below the detection limit

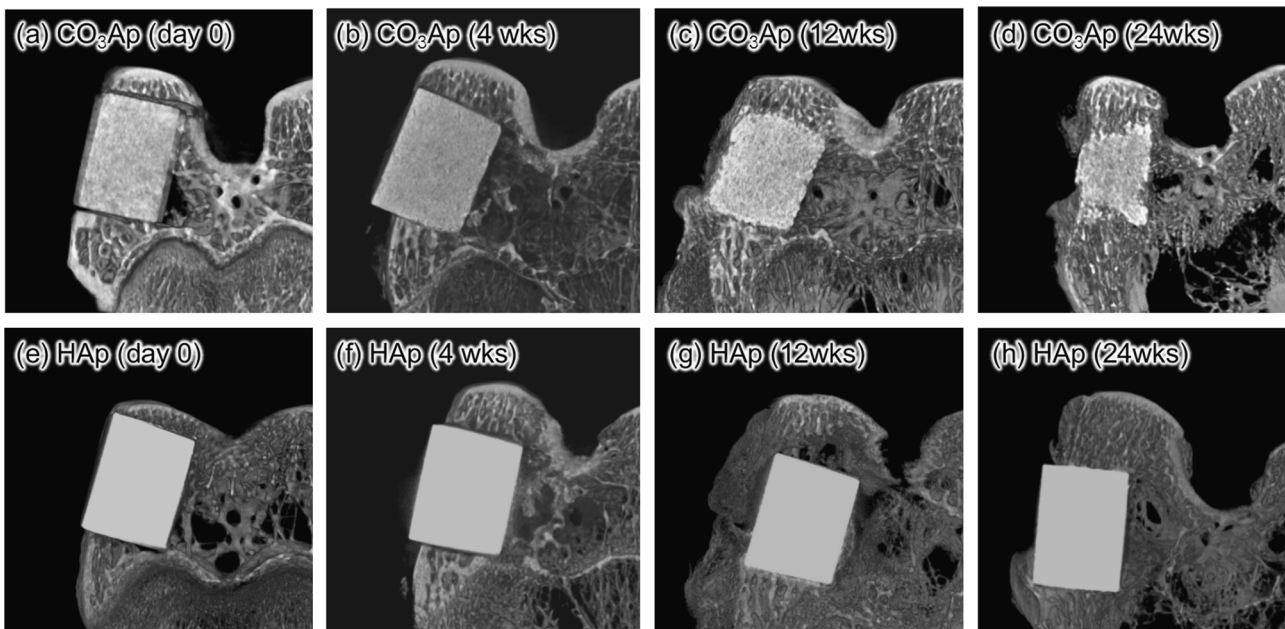


**Fig. 5** Micro-computed tomography (CT) images (side view of the cylindrical block) of CO<sub>3</sub>Ap blocks (**a–d**) and HAp blocks (**e–h**) immediately after implantation (day 0) (**a, e**) and at 4 (**b, f**), 12 (**c, g**), and 24 (**d, h**) weeks after implantation in the rabbits' distal femurs

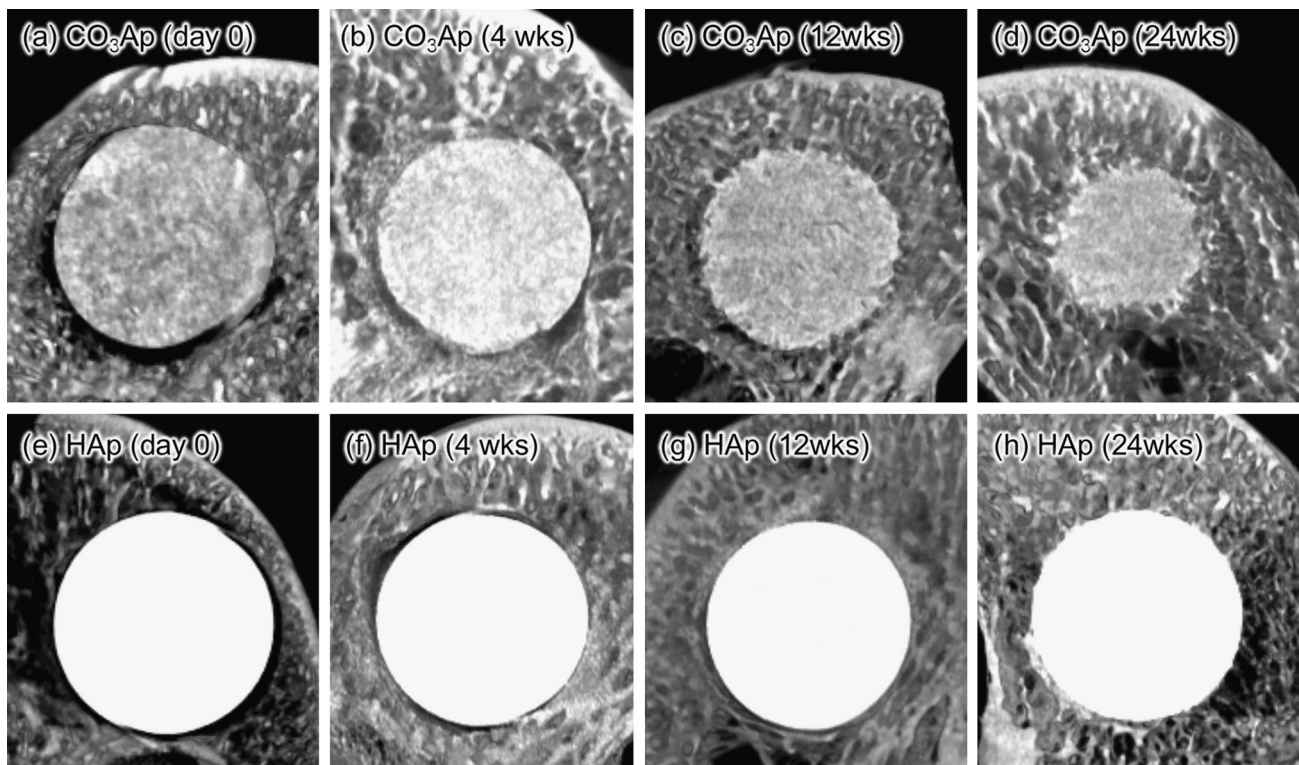


**Fig. 6** Micro-CT sagittal images of the rabbits' distal femurs from a top view of the CO<sub>3</sub>Ap blocks (a–d) and HAp blocks (e–h) immediately after implantation (day 0) (a, e) and at 4 (b, f), 12 (c, g), and 24 (d, h) weeks after implantation in rabbits' distal femurs

words, there was no sign of resorption in the case of sintered HAp.

CO<sub>3</sub>Ap block showed less opacity than the HAp block throughout the experimental period. In contrast to the HAp block, the size of the CO<sub>3</sub>Ap block decreased with increasing time after implantation. At 4 weeks after implantation, the CO<sub>3</sub>Ap block basically maintained its structure, although the edge of the CO<sub>3</sub>Ap block inside the bone became rounded, indicating that the area was being resorbed and replaced with bone. At 12 weeks after implantation, there was much more resorption and replacement than was seen at 4 weeks. All of the CO<sub>3</sub>Ap edges had become rounded. In addition, other surfaces were being resorbed and replaced with bone. As a result, the CO<sub>3</sub>Ap block, which had had a rectangular shape had become more rounded. At 24 weeks after implantation, there was even more resorption of the CO<sub>3</sub>Ap block, and more of it had been replaced with bone. Resorption of the CO<sub>3</sub>Ap block and its replacement with bone seemed to be accelerated when compared with that at the initial stage.

Figure 6 summarizes the micro-CT sagittal images of the rabbits' distal femurs from a top view of the cylindrical block. Gaps were observed between bone and both the HAp and CO<sub>3</sub>Ap blocks at this stage. At 4 weeks, bone had grown to contact the surface of the CO<sub>3</sub>Ap, whereas the gap between the HAp block and bone remained, although it had

decreased. At 12 and 24 weeks, the CO<sub>3</sub>Ap block had decreased in size, whereas the size of the HAp remained the same even at 24 weeks.

Resorption of the CO<sub>3</sub>Ap block is seen more clearly when the sample's structure is picked up from the surrounding bone, as shown in Fig. 7. The CO<sub>3</sub>Ap block became smaller along with the increasing duration of the implantation period whereas the size of the HAp block was the same during the whole experimental period.

Figure 8 shows micro-CT images (side view of the cylindrical block) of the CO<sub>3</sub>Ap (a–d) and HAp (e–h) blocks just after implantation (day 0) (a, e) and at weeks 4 (b, f), 12 (c, g), and 24 (d, h) after implantation in the rabbits' proximal tibias.

Similar to the result for implantation of the HAp block at the femoral bone defect, HAp maintained its structure at 24 weeks postoperatively, even when the HAp block was implanted in the tibial bone defect. In other words, there were no signs of resorption in the case of sintered HAp.

In contrast to the HAp block, when the CO<sub>3</sub>Ap block was implanted at the tibial defect, its size decreased with the increasing implantation period. At 4 weeks after implantation, the CO<sub>3</sub>Ap block basically maintained its structure. However, the edge of the CO<sub>3</sub>Ap block inside the bone had become rounded, indicating that the area was being resorbed and replaced with bone. At 12 weeks after implantation,

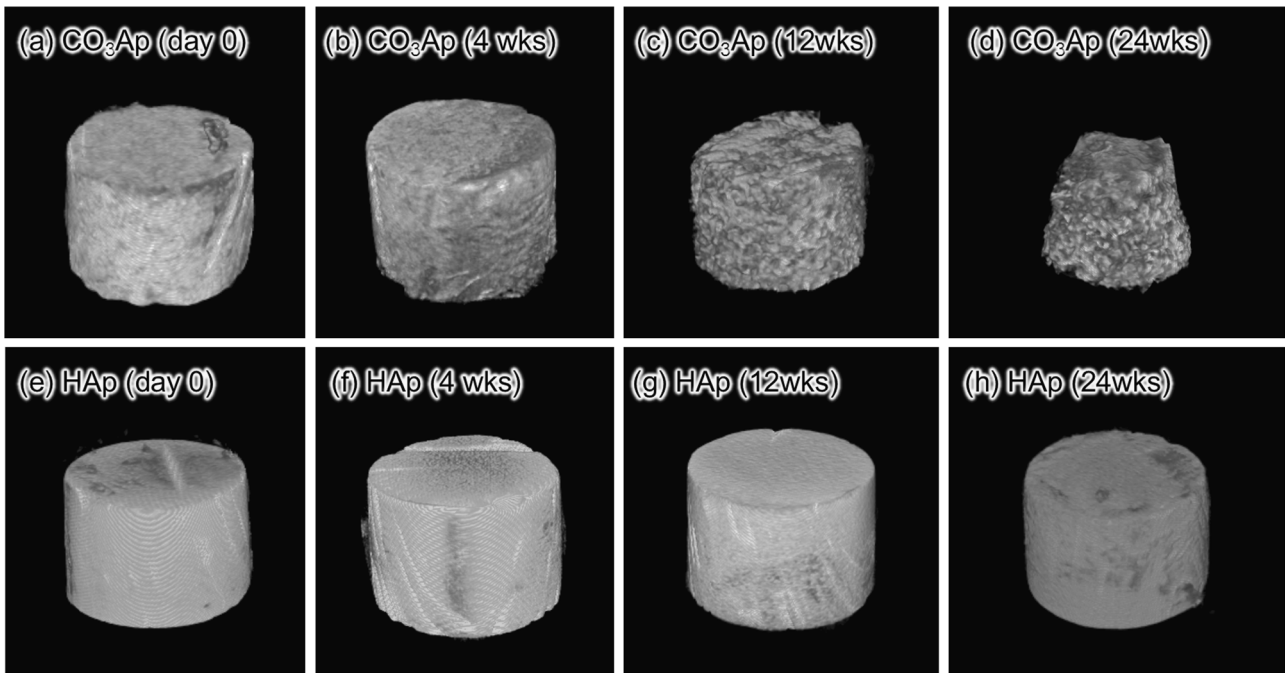


**Fig. 7** Three-dimensional images of the residual volume of the CO<sub>3</sub>Ap blocks (a–d) and HAp blocks (e–h) immediately after implantation (day 0) (a, e) and at 4 (b, f), 12 (c, g), and 24 (d, h) weeks after implantation in rabbits’ distal femurs

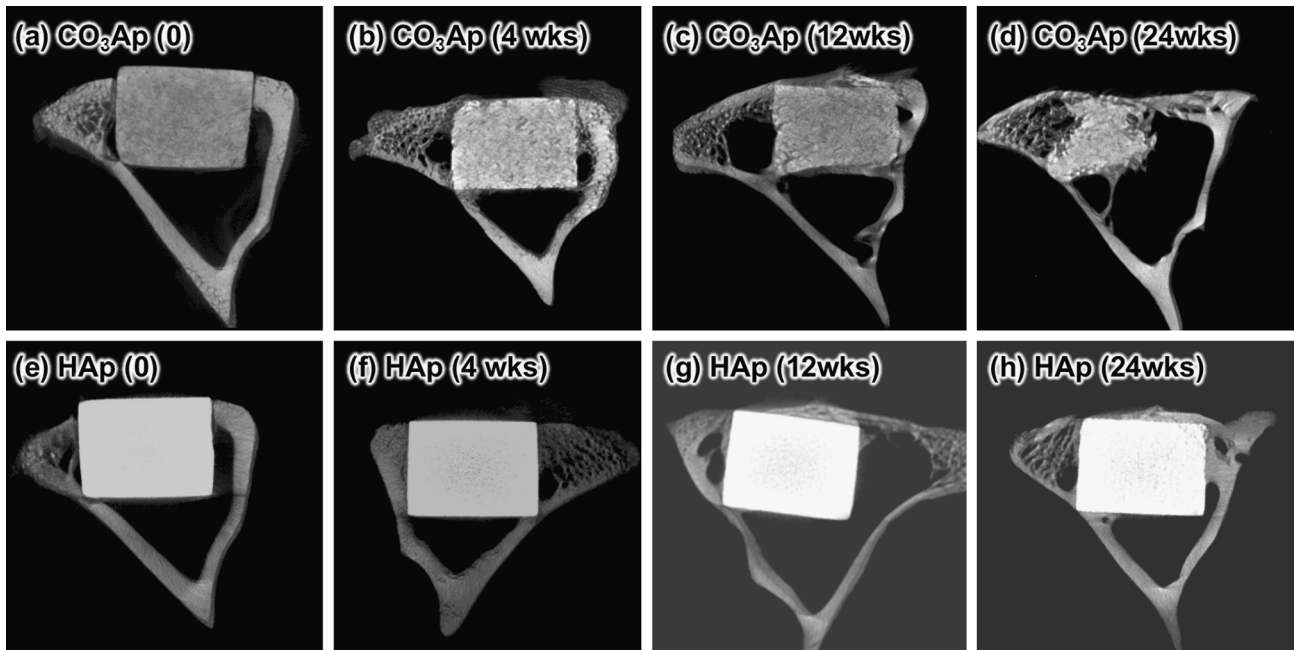


**Fig. 8** Micro-CT images (side view of the cylindrical block) of the CO<sub>3</sub>Ap blocks (a–d) and HAp blocks (e–h) just after implantation (day 0) (a, e) and at 4 (b, f), 12 (c, g), and 24 (d, h) weeks after implantation in the rabbits’ proximal tibiae

resorption and replacement with bone had proceeded in much larger quantities than at 4 weeks. All of the edge of the CO<sub>3</sub>Ap had become rounded. In addition to the edge of the CO<sub>3</sub>Ap block, other surfaces were resorbed and

replaced with bone at this stage. As a result, the CO<sub>3</sub>Ap block, which had been rectangular, was becoming increasingly rounded. At 24 weeks after implantation, there was more resorption of the CO<sub>3</sub>Ap block and replacement with

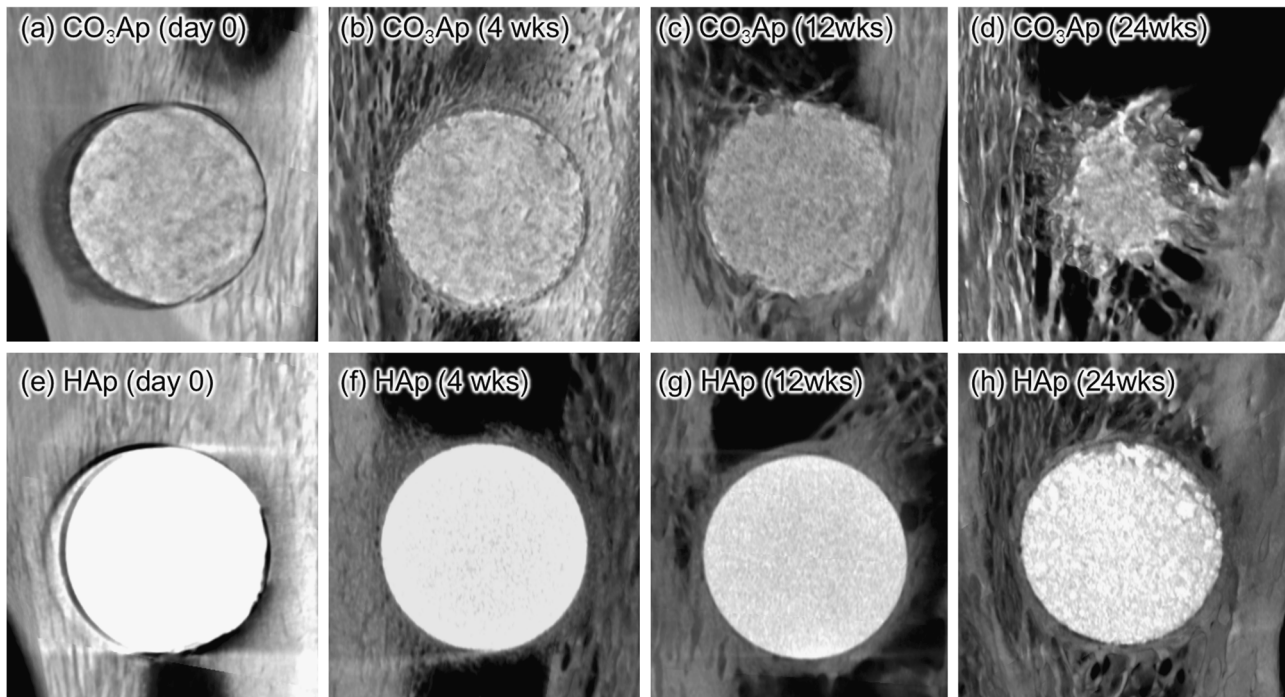


**Fig. 9** Micro-CT sagittal images of the rabbits' proximal tibias from a top view of the CO<sub>3</sub>Ap (a–d) blocks and HAp blocks (e–h) immediately after implantation (day 0) (a, e) and at 4 (b, f), 12 (c, g), and 24 (d, h) weeks after implantation in rabbits' proximal tibias

bone than had been seen at 12 weeks. That is, resorption of the CO<sub>3</sub>Ap block and its replacement with bone seemed to have accelerated when compared with the initial stage.

Figure 9 summarizes micro-CT sagittal images (from top view of a cylindrical block) when the sample was implanted in rabbits' tibial bone defects. A gap was observed between the block and bone at this stage for both HAp and CO<sub>3</sub>Ap blocks. At 4 weeks, however, the bone was in contact with the surface of the CO<sub>3</sub>Ap block, whereas the gap between the HAp block and bone remained although it had decreased somewhat. At 12 and 24 weeks, the CO<sub>3</sub>Ap block had become smaller linearly with the increasing duration of the implantation period. In contrast, the HAp was the same size even at 24 weeks.

Figure 10 shows the images of the remaining tibial CO<sub>3</sub>Ap and HAp blocks at 24 weeks after implantation. Similar to the results when implanted in the femur, CO<sub>3</sub>Ap block became smaller with the increasing implantation period whereas the size of the HAp block was the same during the whole experimental period. Resorption of the CO<sub>3</sub>Ap block was faster at the tibial bone defects than at the femoral bone defects.

Figure 11 shows the resorption rates for the CO<sub>3</sub>Ap and HAp blocks implanted at different sites. Resorption of the CO<sub>3</sub>Ap showed an approximately linear change with passing time regardless of the implantation site. Interestingly, the resorption rate of the CO<sub>3</sub>Ap block in the proximal tibia was significantly faster than that in the distal femur

throughout the post-implantation period. In contrast, the HAp block showed almost no resorption during the post-implantation period regardless of the implantation site.

Resorption of the CO<sub>3</sub>Ap block prepared from a DCPD precursor block showed an approximately linear change throughout the post-implantation period, as shown in Fig. 11.

#### 4 Discussion

Purpose of this study is to evaluate the osteoconductivity and resorbability of CO<sub>3</sub>Ap block fabricated from DCPD block in two different implantation sites (rabbit femoral and tibial defects) by the evaluation using micro-CT. Since we would like to compare the ability of the obtained CO<sub>3</sub>Ap block to clinically used HAp bone substitutes, a sintered HAp was chosen as a control in this experiment.

Both CO<sub>3</sub>Ap and HAp showed good osteoconductivity indicated by micro-CT analysis after 4 weeks implantation (Figs. 5, 6, 8 and 9) regardless of the implantation site. An initial osteoconductivity of CO<sub>3</sub>Ap in femur seemed to be higher than that of HAp because the surrounding bone had grown to contact the edge of CO<sub>3</sub>Ap block whereas the gap between HAp and surrounding bone was remained (Figs. 5 and 6). However, in tibia, the surrounding bone had grown to contact both CO<sub>3</sub>Ap and HAp. For making discussion on osteoconductivity more in detail, a histological evaluation



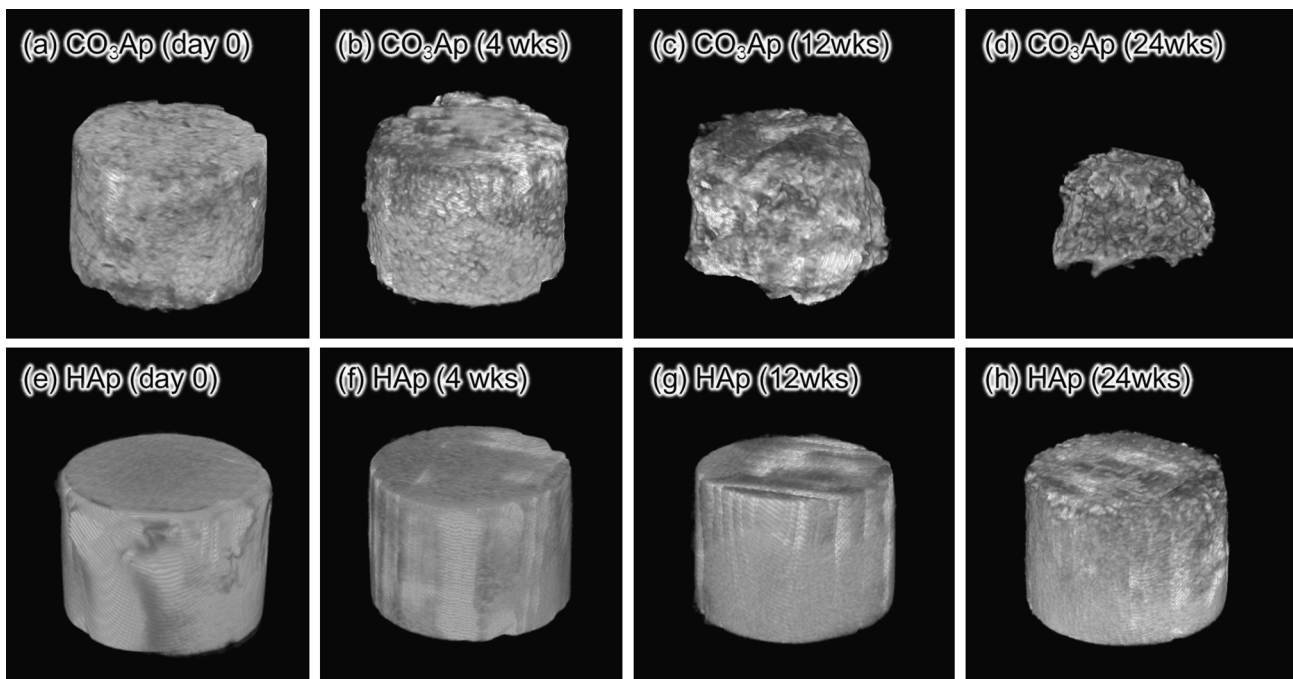


**Fig. 10** Three-dimensional images of the residual volume of the CO<sub>3</sub>Ap blocks (a–d) and HAp blocks (e–h) immediately after implantation (day 0) (a, e) and at 4 (b, f), 12 (c, g), and 24 (d, h) weeks after implantation in rabbits’ proximal tibias

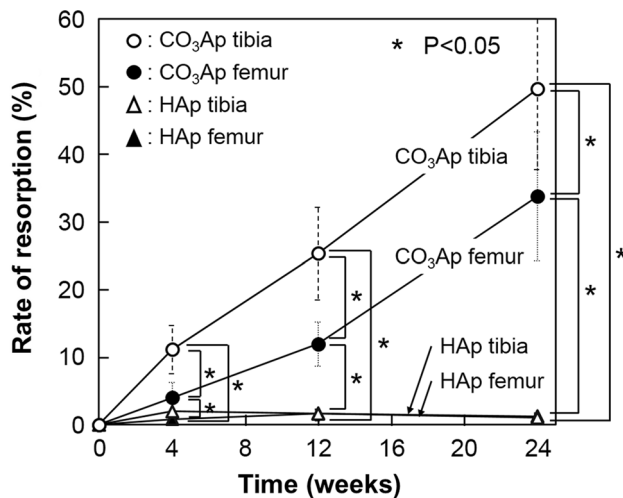


**Fig. 11** Resorption rate (%) for the CO<sub>3</sub>Ap and HAp blocks implanted in different sites of bony tissue (femur and tibia)

in each implantation period must be necessary. Therefore, we will perform the histological evaluation in the near future.

The results obtained by the micro-CT analysis clearly demonstrated that the CO<sub>3</sub>Ap block prepared from a DCPD precursor block was gradually resorbed in the rabbit’s bony defect, whereas the sintered HAp block showed no sign of resorption throughout of post-implantation period. It is thought that the difference in resorption between the CO<sub>3</sub>Ap

and HAp blocks must be due to the different degrees of SSA, porosity, and carbonate content of each specimen as shown in Table 1.

Resorption of the CO<sub>3</sub>Ap block prepared from a DCPD precursor block showed an approximately linear change throughout the post-implantation period, as shown in Fig. 11. At 24 weeks after implantation, resorption rate of the CO<sub>3</sub>Ap block at tibia and femur were about 50% and 34%, respectively. By extrapolation of the results, we estimated that it would take approximately 48 weeks (1 year) in tibia and 72 weeks (1.5 year) in femur to resorb the CO<sub>3</sub>Ap block completely. This resorption is probably due to the osteoclasts, not physical dissolution. It is because, among the calcium phosphates, apatite (including carbonate apatite) is the most thermodynamically stable phase [9]. In fact, we previously reported that CO<sub>3</sub>Ap granules (prepared from the CaCO<sub>3</sub> precursor [9]) and CO<sub>3</sub>Ap granules (derived from the CaSO<sub>4</sub> precursor [12]) were resorbed by osteoclasts and gradually replaced to create new bone. Therefore, we found that CO<sub>3</sub>Ap fabricated through a dissolution–precipitation reaction can be resorbed in a bony defect regardless of differences in the precursors. Although various precursors are available for fabricating CO<sub>3</sub>Ap bone substitute, the resorption rate for CO<sub>3</sub>Ap when using the dissolution–precipitation reaction is thought to be affected by the difference in the precursor’s solubility. The HAp block fabricated using an α-TCP precursor block showed greater porosity than that fabricated using a β-TCP precursor block,

depending on their precursor's solubility [26]. Because osteoclastic resorption may be affected by the porosity of the CO<sub>3</sub>Ap block, the effect of the precursor's difference in resorption of the CO<sub>3</sub>Ap block must be examined as the next research target using the same size specimen but prepared from different precursors, such as CaCO<sub>3</sub>, CaSO<sub>4</sub>, and  $\alpha$ -TCP.

The results obtained in this in vivo evaluation by micro-CT clearly demonstrated that resorption of the CO<sub>3</sub>Ap block was affected by the implantation site. As shown in Figs. 5–11, the metaphyseal site on the proximal tibia showed greater resorption of the CO<sub>3</sub>Ap blocks than the epiphyseal site on the distal femur, suggesting higher osteoclastic activity at the metaphysis. Blood vessel development is greater at the metaphysis than at the epiphysis [27], suggesting that the larger blood supply may contribute to the existence of more osteoclasts and thus greater resorption of the CO<sub>3</sub>Ap block. It might be one of the reasons for the different resorption levels of the CO<sub>3</sub>Ap block between the epiphyseal site of the distal femur and the metaphyseal site of the proximal tibia. Further histologic data for confirming new bone formation and the activities of various cells are necessary to understand the detailed mechanism. Either way, CO<sub>3</sub>Ap blocks showed far better resorption than HAp blocks.

## 5 Conclusions

A CO<sub>3</sub>Ap block prepared from a DCPD precursor block showed good resorption in bone tissue, whereas the sintered HAp block showed almost no resorption 6 months after implantation. The resorption rate of the CO<sub>3</sub>Ap block was faster at the metaphysis of the proximal tibia than at the epiphysis of the distal femur. Based on our results, complete resorption for a disk-shaped CO<sub>3</sub>Ap block (6 mm diameter, 4 mm high) was estimated to be approximately 1–1.5 years. Resorption of a CO<sub>3</sub>Ap block was probably achieved by osteoclasts although it should be confirmed by the histological evaluation in the future.

**Acknowledgements** The Strategic Promotion of Innovative Research and Development Program from the Japan Agency for Medical Research and Development (16im0502004h) partially supported this research. This work was also partially supported by JSPS KAKENHI (Grant Number 15H05035).

**Conflict of interest** The authors declare that they have no competing interests.

## References

- Moore WR, Graves SE, Bain GI. Synthetic bone graft substitutes. *ANZ J Surg.* 2001;71:354–61.
- Brekke JH, Toth JM. Principles of tissue engineering applied to programmable osteogenesis. *J Biomed Mater Res.* 1998;43:380–98.
- Nasr HF, Aichelmann-Reidy ME, Yukna RA. Bone and bone substitutes. *Periodontol* 2000. 1999;19:74–86.
- Taylor BC, French BG, Fowler TT, Russell J, Poka A. Induced membrane technique for reconstruction to manage bone loss. *J Am Acad Orthop Surg.* 2012;20:142–50.
- El Deeb M, Roszkowski M. Hydroxylapatite granules and blocks as an extracranial augmenting material in rhesus monkeys. *J Oral Maxillofac Surg.* 1988;46:33–40.
- Kent JN, Zide MF, Kay JF, Jarcho M. Hydroxylapatite blocks and particles as bone graft substitutes in orthognathic and reconstructive surgery. *J Oral Maxillofac Surg.* 1986;44:597–605.
- Jarcho M. Calcium phosphate ceramics as hard tissue prosthetics. *Clin Orthop Relat Res* 1981;157:259–78.
- Bohner M, Galea L, Doebelin N. Calcium phosphate bone graft substitutes: failures and hopes. *J Eur Ceramic Soc.* 2012;32:2663–71.
- Ishikawa K. Bone substitute fabrication based on dissolution-precipitation reactions. *Materials.* 2010;3:1138–55.
- Sunouchi K, Tsuru K, Maruta M, Kawachi G, Matsuya S, Terada Y, Ishikawa K. Fabrication of solid and hollow carbonate apatite microspheres as bone substitutes using calcite microspheres as a precursor. *Dent Mater J.* 2012;31:549–57.
- Nomura S, Tsuru K, Maruta M, Matsuya S, Takahashi I, Ishikawa K. Fabrication of carbonate apatite blocks from set gypsum based on dissolution-precipitation reaction in phosphate-carbonate mixed solution. *Dent Mater J.* 2014;33:166–72.
- Ayukawa Y, Suzuki Y, Tsuru K, Koyano K, Ishikawa K. Histological comparison in rats between carbonate apatite fabricated from gypsum and sintered hydroxyapatite on bone remodeling. *Biomed Res Int.* 2015;2015:579541
- Wakae H, Takeuchi A, Udoh K, Matsuya S, Munar ML, LeGeros RZ, et al. Fabrication of macroporous carbonate apatite foam by hydrothermal conversion of  $\alpha$ -tricalcium phosphate in carbonate solutions. *J Biomed Mater Res Part A.* 2008;87A:957–63.
- Takeuchi A, Munar ML, Wakae H, Maruta M, Matsuya S, Tsuru K, Ishikawa K. Effect of temperature on crystallinity of carbonate apatite foam prepared from  $\alpha$ -tricalcium phosphate by hydrothermal treatment. *Biomed Mater Eng.* 2009;19:205–11.
- Sugiura Y, Tsuru K, Ishikawa K. Fabrication of carbonate apatite foam based on the setting reaction of  $\alpha$ -tricalcium phosphate foam granules. *Ceramics Int.* 2016;42:204–10.
- LeGeros RZ. Calcium phosphates in oral biology and medicine. In: Myers HM, editor. *Monographs in oral science* Vol. 15S. Basel: KARGER; 1991. p. 108–29. ISBN: 978-3-8055-5236-3
- Tsuru K, Kanazawa M, Yoshimoto A, Nakashima Y, Ishikawa K. Fabrication of carbonate apatite block through dissolution-precipitation reaction using calcium hydrogen phosphate dihydrate block as a precursor. *Materials.* 2017;10(4):374.
- Mirtchi AA, Lemaitre J, Terao N. Calcium phosphate cements: study of the  $\beta$ -tricalcium phosphate-monocalcium phosphate system. *Biomaterials.* 1989;10:475–80.
- Mirtchi AA, Lemaitre J, Munting E. Calcium phosphate cements: action of setting regulators on the properties of the  $\beta$ -tricalcium phosphate cements. *Biomaterials.* 1989;10:634–8.
- Bohner M, Lemaitre J. Hydraulic properties of tricalcium phosphate-phosphoric acid-water mixtures. In: Duran P, Fernandez JF, editors. *Third Euro-Ceramics*. Castellon de la Plana, Spain: Faenza Editrice Iberica S.L.; 1993. p. 95–100.
- Suresh S. Theoretical studies of solid state dielectric parameters of hydroxyapatite. *Mater Phys Mech.* 2012;14:145–51.
- Chai YC, Kerckhofs G, Roberts SJ, Van Bael S, Schepers E, Vleugels J, Luyten FP, Schrooten J. Ectopic bone formation by 3D porous calcium phosphate-Ti6Al4V hybrids produced by perfusion electrodeposition. *Biomaterials.* 2012;33:4044–58.

23. Fowler BO. Infrared studies of apatites. I. Vibrational assignments for calcium, strontium, and barium hydroxyapatites utilizing isotopic substitution. *Inorg Chem.* 1974;13:194–207.
24. Elliott JC, Holcomb DW, Young RA. Infrared determination of the degree of substitution of hydroxyl by carbonate ions in human dental enamel. *Calcif Tissue Int.* 1985;37:372–5.
25. Rey C, Collins B, Goehl T, Dickson IR, Glimcher MJ. The carbonate environment in bone mineral: a resolution-enhanced Fourier transform infrared spectroscopy study. *Calcif Tissue Int.* 1989;45:157–64.
26. Ahmad N, Tsuru K, Munar ML, Maruta M, Matsuya S, Ishikawa K. Effect of precursor's solubility on the mechanical property of hydroxyapatite formed by dissolution-precipitation reaction of tricalcium phosphate. *Dent Mater J.* 2012;31:995–1000.
27. Brookes M, Revell WJ. *Blood Supply of Bone.* London: Springer; 1998.